

Dynamical properties of the crust of neutron stars derived from realistic NN interactions

P. Grygorov, P. Gögelein and H. Mütter

Institut für Theoretische Physik,

Universität Tübingen,

D-72076 Tübingen, Germany

The mean free path of neutrino in charged and neutral current reactions is calculated for inhomogeneous nuclear matter which is expected to appear in the crust of neutron stars. The relevant cross section depends on Fermi and Gamow-Teller strength distributions, which are derived from the large-scale shell model calculations within the self-consistent Skyrme-Hartree-Fock approach and in a relativistic mean-field model. The inhomogeneous nuclear matter is described in terms of cubic Wigner-Seitz cells, which allows for a microscopic description of the structures in the so-called pasta phase of nuclear configurations and provides a smooth transition to the limit of homogeneous matter. The influence of pasta phase, its microscopical structure and geometrical shapes on neutrino propagation is considered.

I. INTRODUCTION

The transport properties of neutrino play an essential role in the physics of supernovae core collapse and in the evolution of the newly born neutron stars. The most important ingredient of neutrino propagation calculations is the neutrino opacity in a wide range of densities. Both the charged current (CC) absorption and neutral current (NC) scattering reactions are important sources of the neutrino opacity. In earlier works on neutrino interactions with the homogeneous nuclear matter the noninteracting baryons were considered [1]. Later the strong interaction was taken into account both in the non-relativistic and relativistic calculations (see, e.g., [2, 3, 4, 5, 6, 7] and ref. therein). It was shown that the neutrino opacities of interacting matter may significantly be altered from those for the noninteracting case [4]. However, the use of homogeneous matter is a good approximation, while the existence of the stable quasi-nuclei in the crust of neutron stars is energetically favorable

and must be taken into account.

At low densities, the nuclei in matter are expected to form the Coulomb lattice embedded in the neutron sea, that minimizes the Coulomb repulsion between the protons. With increase of density the nuclear pasta structures occur and the stable nuclear shape may change form from spherical droplet to rod, slab, tube and bubble shapes [8]. Roughly speaking, the favorable nuclear shape is determined by a balance between the surface and Coulomb energies. In the following under "pasta phase" we will assume quasi-nuclear structures with spherical as well as non-spherical shape, which are embedded in a neutron sea.

Various attempts have been made to describe the ground-state structure of pasta phase based on Thomas-Fermi approximation [9], Quantum Molecular Dynamics [10, 11, 12, 13], Hartree-Fock and Relativistic Mean-Field calculations (RMF) within the Wigner-Seitz (WS) cell approximation [16, 17, 18]. Later the dynamical properties of pasta such as the response function and neutrino mean free path (NMFP) were investigated [10, 13, 14, 15]. It was found that the coherent scattering of neutrinos on inhomogeneous matter significantly reduces the mean free path. The collective modes in neutron rich skin of pasta were also calculated in a random phase approximation by using spherical Skyrme-Hartree-Fock (SHF) method [19]. It was shown the appearance of the super-giant resonance mode at low excitation energy, which may affect the specific heat of the crust of neutron stars.

The calculation of the NMFP in pasta phase presented in this work is based on Hartree-Fock calculations in cubic WS cell [16, 17, 18], which allows for the description of non-spherical quasi-nuclear structures such as rods or slabs and contains the limit of homogeneous matter in a natural way. The self-consistent calculations are performed for β -stable matter in a density range for which the quasi-nuclear structures discussed above are expected to appear. For the nuclear Hamiltonian we consider Skyrme forces (SLy4) but also perform calculations within the relativistic mean-field (Hartree) approximation. The stability of the pasta phase with increase of the temperature is also discussed.

The NMFP is extracted from the relevant cross sections of neutrino on different pasta structures. We pay special attention to the dependence of our results on the internal structure of the pasta phase and its geometrical shapes. The mean free paths obtained from these inhomogeneous structures are compared with those calculated for homogeneous nuclear matter at the same global density, thus one can estimate the influence of the inhomogeneous phase on the propagation of neutrinos.

After this introduction the details of Skyrme-Hartree-Fock approach with pairing will be outlined and a method to calculate the NMFP will be reviewed in section 2. In section 3 we discuss the density dependent relativistic mean-field (DDRMF) model. The numerical results are discussed in section 4 and the final section 5 contains the main conclusions.

II. SKYRME-HARTREE-FOCK CALCULATIONS

A. Energy functional

The Skyrme-Hartree-Fock approach has frequently been described in the literature [20, 21, 22, 23]. Therefore we will outline here only a few basic equations, which will define the nomenclature. The Skyrme model is defined in terms of an energy density $\mathcal{H}(\mathbf{r})$, which can be split into various contributions[21, 24]

$$\mathcal{H} = \mathcal{H}_K + \mathcal{H}_0 + \mathcal{H}_3 + \mathcal{H}_{\text{eff}} + \mathcal{H}_{\text{fin}} + \mathcal{H}_{\text{so}} + \mathcal{H}_{\text{Coul}}, \quad (1)$$

where \mathcal{H}_K is the kinetic energy term, \mathcal{H}_0 a zero range term, \mathcal{H}_3 a density dependent term, \mathcal{H}_{eff} an effective mass term, \mathcal{H}_{fin} a finite range term and \mathcal{H}_{so} a spin-orbit term. These terms are given by

$$\begin{aligned} \mathcal{H}_K &= \frac{\hbar^2}{2m} \tau, \\ \mathcal{H}_0 &= \frac{1}{4} t_0 [(2 + x_0) \rho^2 - (2x_0 + 1)(\rho_p^2 + \rho_n^2)], \\ \mathcal{H}_3 &= \frac{1}{24} t_3 \rho^\alpha [(2 + x_3) \rho^2 - (2x_3 + 1)(\rho_p^2 + \rho_n^2)], \\ \mathcal{H}_{\text{eff}} &= \frac{1}{8} [t_1(2 + x_1) + t_2(2 + x_2)] \tau \rho \\ &\quad + \frac{1}{8} [t_2(2x_2 + 1) - t_1(2x_1 + 1)] [\tau_p \rho_p + \tau_n \rho_n], \\ \mathcal{H}_{\text{fin}} &= -\frac{1}{32} [3t_1(2 + x_1) - t_2(2 + x_2)] \rho \Delta \rho \\ &\quad + \frac{1}{32} [3t_1(2x_1 + 1) + t_2(2x_2 + 1)] [\rho_p \Delta \rho_p + \rho_n \Delta \rho_n], \\ \mathcal{H}_{\text{so}} &= -\frac{1}{2} W_0 [\rho \nabla \mathbf{J} + \rho_p \nabla \mathbf{J}_p + \rho_n \nabla \mathbf{J}_n]. \end{aligned} \quad (2)$$

The coefficients t_i , x_i , W_0 , and α are the parameters of a generalized Skyrme force [25]. The imaginary time step was used to solve the Hartree-Fock equations [16, 17, 26]. The calculations were performed in a cubic Wigner-Seitz cell with a size of typically 20 fm for charge neutral matter containing protons, neutrons and electrons in β -equilibrium. Pairing corre-

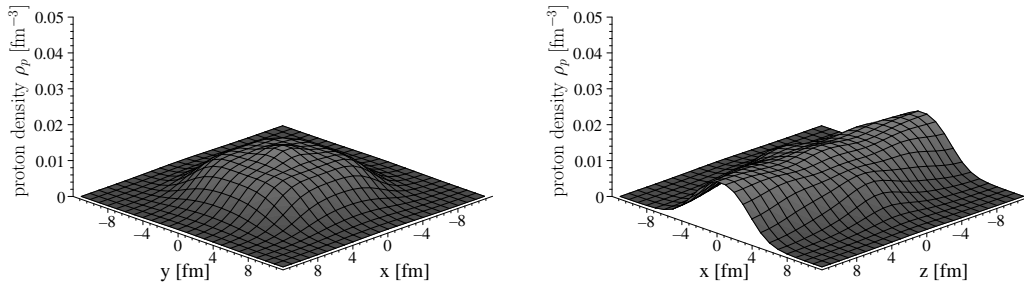


FIG. 1: Profiles for the proton density distribution forming a rod-structure at a density of 0.0625 fm^{-3} .

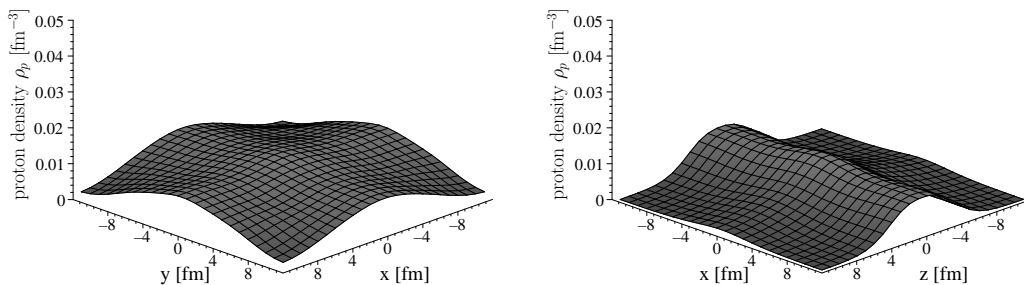


FIG. 2: Profiles for the proton density distribution forming a slab-structure at a density of 0.0775 fm^{-3} .

lations are included in terms of the BCS approximation by assuming a density-dependent zero-range pairing force, which has been used in earlier calculations [16, 18, 27].

Figure 1 displays a typical example for the density profile of the proton distribution. At the global nucleon density of 0.0625 fm^{-3} we obtain a quasi-nuclear structure which can be characterized as rods along the z -axis. At a density of 0.0775 fm^{-3} the variational Hartree-Fock leads to a quasi-nuclear structure, which can be characterized as a set of parallel slabs. In figure 2, which shows the proton density distribution at this density, we have chosen the orientation of the coordinates such that these slabs are orthogonal to the z -axis.

The single-particle energies and wave functions for protons and neutrons resulting from such Hartree-Fock calculations were used to evaluate the NMFP by using the method outlined in the following subsection.

B. Neutrino mean free path in Skyrme-Hartree-Fock model

The matrix element for the neutrino-nucleon reactions $\nu + n \rightarrow \nu + n$ ($\nu + n \rightarrow p + e$) is given by

$$M = \frac{G_F C}{\sqrt{2}} J_\mu j^\mu, \quad (3)$$

where

$$J_\mu = i\bar{u}_{n(p)}(V\gamma_\mu + A\gamma_\mu\gamma_5)u_n, \quad (4)$$

$$j^\mu = -i\bar{u}_\nu\gamma^\mu(1 - \gamma_5)u_{\nu(e)} \quad (5)$$

are hadronic and leptonic currents, respectively. The parameters A, V must be replaced by the respective values of coupling constants and C stands for the Cabbibo factor in the charged-current reaction [28]. The total cross section can be written as

$$\sigma = \sum_f p_{\nu(e)} E_{\nu(e)} \frac{1}{2} \int_{-1}^1 d(\cos \vartheta) |\overline{M}|^2, \quad (6)$$

$$|\overline{M}|^2 = \frac{G_F^2 C^2}{\pi} \left[V^2 (1 + \cos \vartheta) |M_1|^2 + A^2 (1 - \frac{1}{3} \cos \vartheta) |M_2|^2 \right], \quad (7)$$

$$M_1 = \langle \varphi_4 | e^{i\vec{q}\vec{r}} | \varphi_2 \rangle, \quad M_2 = \langle \varphi_4 | \vec{\sigma} e^{i\vec{q}\vec{r}} | \varphi_2 \rangle, \quad (8)$$

where within this non-relativistic approach we neglect the lower components in Dirac spinors $u \simeq \begin{pmatrix} \varphi \\ 0 \end{pmatrix}$. In the charged current reaction the influence of the Coulomb field on the outgoing electron can be taken into account by multiplying the cross section by the Fermi function $F(Z_f, E_e)$ [29]. For this reaction M_1 and M_2 stand for the Fermi and Gamow-Teller matrix elements, respectively. The integration is performed over the spatial angle ϑ between the momenta of incoming and the outgoing leptons. The single-particle wave functions $\varphi(\vec{r})$ and single-particle energies ε_f (ε_i) are obtained from the solution of the HF equations. Note that these single-particle energies enter (6) as the energy for the outgoing lepton is defined as

$$E_{\nu(e)} = E_\nu^{in} + \varepsilon_i - \varepsilon_f,$$

where E_ν^{in} is the energy of the incoming neutrino.

The formalism described so far is appropriate for the neutrino-nucleus interaction. With some extensions it may also be used to evaluate the interaction of neutrinos with the quasi-nuclear structures in the crust of neutron stars. Unlike spherical nuclei and the case of the

droplet phase, the cross section of neutrino on rods and slabs, generally speaking, depends on the spatial orientation of momentum transfer \vec{q} in (8), since the density distributions of rod and slab phases are non spherical, as it is shown on figures 1,2. The precise averaging over all possible mutual orientations of vectors \vec{q} and \vec{r} requires additional numerical efforts. Thus, in order to reduce this effort we considered three particular cases, with the vector \vec{q} along the direction of the x, y and z-axis. Doing so, we determine the averaged cross section as

$$\sigma = \frac{1}{3}(\sigma_x + \sigma_y + \sigma_z), \quad (9)$$

where $\sigma_{x(y,z)}$ represents the cross section calculated for the momentum transfer along $x(y,z)$ -axis.

In contrast to a finite nucleus, the WS cell of the inhomogeneous nuclear matter contains a large number of unbound neutrons, which give nonzero contribution to the total cross section. Thus, the cross section consists of two parts: the cross section due to the interaction with the nucleons bound in the quasi-nuclear structure and the cross section due to the interaction with unbound neutrons. Therefore, one can consider (6) as a cross section of neutrinos with all nucleons in a given volume V_{cell} of a WS cell. The reverse NMFP can then be written as

$$\frac{1}{\lambda} = \frac{\sigma}{V_{cell}}. \quad (10)$$

Another important distinction of pasta structures in the crust of neutron stars from the finite, isolated nuclei consists in the existence of the electron sea in the volume of the WS cell. Therefore the nonzero chemical potential of electrons must be taken into account in the evaluation of charged current reactions by a blocking of final states for electrons with energies below the respective Fermi energy μ_e .

III. RELATIVISTIC MEAN-FIELD CALCULATIONS

In order to test the sensitivity of the results on the underlying nuclear model and the choice of the NN interaction we also investigated the dynamical properties of inhomogeneous nuclear matter evaluated within a relativistic mean-field (Hartree) approximation by using a model of density-dependent meson-nucleon coupling constants. The parameterization of these constants has been fitted to reproduce the properties of the nucleon self-energy evaluated in Dirac-Brueckner-Hartree-Fock (DBHF) calculations of asymmetric nuclear matter

but has also been adjusted to provide a good description for bulk properties of finite nuclei [30, 31, 32, 33]. The density-dependent relativistic mean-field (DDRMF) approach has also been used to describe the properties of inhomogeneous nuclear matter in the crust of neutron stars [18].

A. Density dependent relativistic mean-field approach

The relativistic mean-field (RMF) approach is an effective field theory of interacting mesons and nucleons. The Lagrangian density consists of three parts: the free baryon Lagrangian density \mathcal{L}_B , the free meson Lagrangian density \mathcal{L}_M and the interaction Lagrangian density \mathcal{L}_{int} :

$$\mathcal{L} = \mathcal{L}_B + \mathcal{L}_M + \mathcal{L}_{\text{int}}, \quad (11)$$

which take the explicit form

$$\begin{aligned} \mathcal{L}_B &= \bar{\Psi} (i\gamma_\mu \partial^\mu - M) \Psi, \\ \mathcal{L}_M &= \frac{1}{2} \sum_{\iota=\sigma,\delta} \left(\partial_\mu \Phi_\iota \partial^\mu \Phi_\iota - m_\iota^2 \Phi_\iota^2 \right) \\ &\quad - \frac{1}{2} \sum_{\kappa=\omega,\rho,\gamma} \left(\frac{1}{2} F_{(\kappa)\mu\nu} F_{(\kappa)}^{\mu\nu} - m_\kappa^2 A_{(\kappa)\mu} A_{(\kappa)}^\mu \right), \\ \mathcal{L}_{\text{int}} &= -g_\sigma \bar{\Psi} \Phi_\sigma \Psi - g_\delta \bar{\Psi} \boldsymbol{\tau} \boldsymbol{\Phi}_\delta \Psi \\ &\quad - g_\omega \bar{\Psi} \gamma_\mu A_{(\omega)}^\mu \Psi - g_\rho \bar{\Psi} \boldsymbol{\tau} \gamma_\mu \mathbf{A}_{(\rho)}^\mu \Psi \\ &\quad - e \bar{\Psi} \gamma_\mu \frac{1}{2} (1 + \tau_3) A_{(\gamma)}^\mu \Psi, \end{aligned} \quad (12)$$

with the field strength tensor $F_{(\kappa)\mu\nu} = \partial_\mu A_{(\kappa)\nu} - \partial_\nu A_{(\kappa)\mu}$ for the vector mesons. In the above Lagrangian density the nucleon field consisting of Dirac-spinors in isospin space is denoted by Ψ and the nucleon rest mass by $M = 938.9$ MeV. The scalar meson fields are Φ_σ and $\boldsymbol{\Phi}_\delta$, the vector meson fields $A_{(\omega)}$ and $\mathbf{A}_{(\rho)}$. The mesons have rest masses m_κ for each meson κ and couple to the nucleons with the strength of the coupling constants g_κ , which depend on a density of the nucleon field Ψ . A very convenient parameterization for this density dependence has been given in [32].

The numerical procedure to solve the Dirac equation in the cubic WS cell is the same as in [16, 17, 18]. Pairing correlations are included in terms of the BCS approximation assuming a density dependent zero-range pairing force, which has already been discussed.

The resulting single-particle energies and spinors were used in the calculation of NMFP as described in the next Subsection.

B. Neutrino mean free path in relativistic mean-field model

First, let us consider the charged current reaction. Here we will exploit the most general form for the nucleonic current, which is allowed due to the Lorentz, parity and isospin invariances [28]

$$J_\mu^{CC} = i\bar{\psi}_p[F_1^v(q^2)\gamma_\mu + F_2^v(q^2)\sigma_{\mu\nu}q_\nu + F_A(q^2)\gamma_5\gamma_\mu - iF_p(q^2)\gamma_5q_\mu]\psi_n, \quad (13)$$

where F_1^v and F_2^v are isovector electromagnetic formfactors, F_A is the axial-vector formfactor, F_p is the induced pseudoscalar formfactor. Following the common practice we ignore the contribution of the second-class currents. The leptonic current has the same structure as in (5). Analogously to (3), (7) the averaged squared matrix element for the charged current reaction can be written in the form

$$\begin{aligned} |\overline{M}|^2 = & \frac{G_F^2 C^2}{2} [|\mathcal{M}_1|^2 (1 - \frac{p_l}{3E_l} \cos \vartheta) + |\mathcal{M}_2|^2 (1 + \frac{p_l}{E_l} \cos \vartheta) \\ & + |\mathcal{M}_3|^2 (p_l^2 + E_\nu^2 - 2p_l E_\nu \cos \vartheta - \frac{p_l^3}{3E_l} \cos \vartheta - \frac{p_l}{3E_l} E_\nu^2 \cos \vartheta + \frac{2p_l^2}{3E_l} E_\nu) \\ & + |\mathcal{M}_4|^2 \frac{p_l}{E_l} ((p_l^2 + E_\nu^2) \cos \vartheta - 2E_l E_\nu \cos \vartheta + p_l E_l + \frac{E_l}{p_l} E_\nu^2 - 2p_l E_\nu)], \end{aligned} \quad (14)$$

where

$$\begin{aligned} \mathcal{M}_1 &= F_1 \bar{\psi}_p \vec{\gamma} \psi_n + F_A \bar{\psi}_p \gamma_5 \vec{\gamma} \psi_n, \\ \mathcal{M}_2 &= F_1 \bar{\psi}_p \gamma_0 \psi_n + F_A \bar{\psi}_p \gamma_5 \gamma_0 \psi_n - iF_p \bar{\psi}_p \gamma_5 q_0 \psi_n, \\ \mathcal{M}_3 &= F_2 \bar{\psi}_p \vec{\Sigma} \psi_n, \\ \mathcal{M}_4 &= F_p \bar{\psi}_p \gamma_5 \psi_n, \end{aligned}$$

and

$$\vec{\Sigma} = \begin{pmatrix} \vec{\sigma} & 0 \\ 0 & \vec{\sigma} \end{pmatrix}.$$

Dirac spinors ψ and the respective single-particle energies are obtained from the solution of the Dirac equation [18].

The hadronic part of the neutral current involves additionally isoscalar electromagnetic form factors F_1^s and F_2^s , so that

$$\begin{aligned} J_\mu^{NC} = & \frac{i}{2} \bar{\psi}_n [F_A(q^2) \gamma_5 \gamma_\mu - i F_p(q^2) \gamma_5 q_\mu \\ & + (1 - 2 \sin^2 \theta_W) (F_1^v(q^2) \gamma_\mu + F_2^v(q^2) \sigma_{\mu\nu} q_\nu) \\ & - 2 \sin^2 \theta_W (F_1^s(q^2) \gamma_\mu + F_2^s(q^2) \sigma_{\mu\nu} q_\nu)] \psi_n, \end{aligned} \quad (15)$$

where θ_W is the Weinberg angle. The respective matrix element for this reaction looks like

$$\begin{aligned} |\overline{M}|^2 = & \frac{G_F^2}{8} [|\mathcal{N}_1|^2 (1 - \frac{1}{3} \cos \vartheta) + |\mathcal{N}_2|^2 (1 + \cos \vartheta) \\ & + |\mathcal{N}_3|^2 (E_\nu'^2 + E_\nu^2 - 2 E_\nu E_\nu' \cos \vartheta - \frac{1}{3} E_\nu'^2 \cos \vartheta - \frac{1}{3} E_\nu^2 \cos \vartheta + \frac{2}{3} E_\nu E_\nu'^2) \\ & + |\mathcal{N}_4|^2 (E_\nu - E_\nu')^2 (1 + \cos \vartheta)], \end{aligned} \quad (16)$$

where

$$\begin{aligned} \mathcal{N}_1 &= ((1 - 2 \sin^2 \theta_W) F_1^v - 2 \sin^2 \theta_W F_1^s) \bar{\psi}_n \vec{\gamma} \psi_n + F_A \bar{\psi}_n \gamma_5 \vec{\gamma}, \\ \mathcal{N}_2 &= -F_A \bar{\psi}_n \gamma_5 \gamma_0 \psi_n - ((1 - 2 \sin^2 \theta_W) F_1^v - 2 \sin^2 \theta_W F_1^s) \bar{\psi}_n \psi_n + i F_P \bar{\psi}_n \gamma_5 \psi_n, \\ \mathcal{N}_3 &= ((1 - 2 \sin^2 \theta_W) F_2^v - 2 \sin^2 \theta_W F_2^s) \bar{\psi}_n \vec{\Sigma} \psi_n, \\ \mathcal{N}_4 &= F_P \bar{\psi}_n \gamma_5 \psi_n. \end{aligned}$$

Substituting (14) and (16) in (6) one obtains the mean free path of neutrinos in relativistic mean-field model for charged and neutral current reactions, respectively.

IV. RESULTS AND DISCUSSIONS

Before we start the discussion of the transport properties of neutrinos in the crust of neutron stars let us review some details of self-consistent Hartree-Fock and relativistic mean-field calculations. For all the results presented in this manuscript a temperature $T = 1$ MeV was considered. This temperature is high enough to take into account some effects of finite temperatures and low enough to maintain the pairing correlations and stable quasi-nuclear structures. If the temperature rises, the pasta phase structures become smoother and at some critical temperature they disappear. For the Skyrme-Hartree-Fock approach this critical temperature is around 5 MeV and 10 MeV for slab and rod structures, respectively, while the droplet structure disappears at a temperature higher than 15 MeV. Thus, the spherically

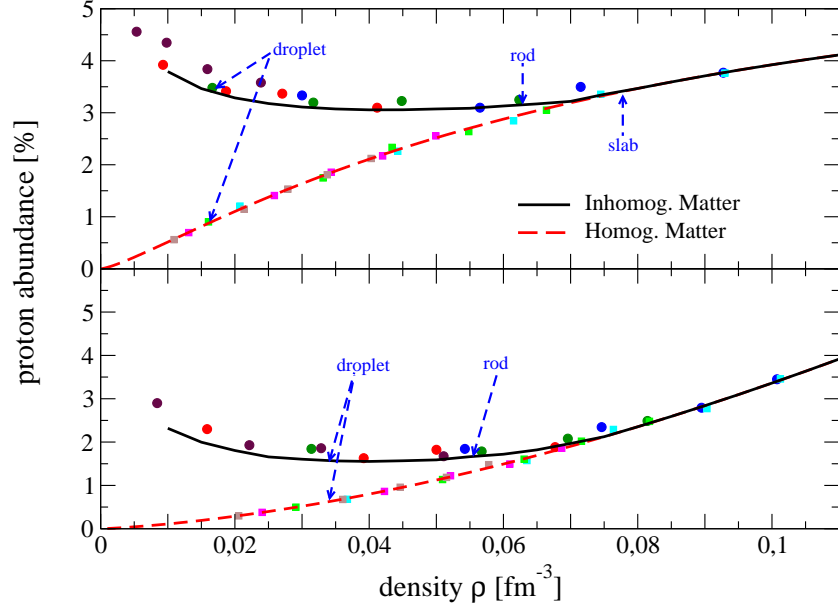


FIG. 3: Proton abundance in the case of uniform matter (dashed line) and pasta phase (solid line). The symbols refer to specific calculations, whereas the lines have been added to guide the eye. The results for Skyrme-Hartree-Fock calculations are shown in the upper panel and the relativistic mean-field results in the lower one. The dashed arrows indicate typical densities leading to pasta structures of droplet, rod and slab shape.

symmetric droplet phase will play the main role in different simulations containing the temperature evolution. Employing the relativistic approach the pasta phase structures turn out to be less stable and even the droplet structures disappear at a temperature of $T = 10$ MeV.

For temperatures below 1 MeV and global densities below 0.08 fm^{-3} the variational calculations yield structures with inhomogeneous density distributions (see figures 1 and 2). Comparing the spectra of single-particle energies obtained for the homogeneous and inhomogeneous solutions one observes that the single-particle energies for the localized states are more deeply bound than the corresponding single-particle states for the homogeneous approach. In the β -equilibrium all proton states are localized and therefore tend to have more attractive single-particle energies in the inhomogeneous as compared to the homogeneous density calculation. The variational calculations allowing for pasta structure yield larger proton fractions than obtained for the β -equilibrium of homogeneous matter at the same global density.

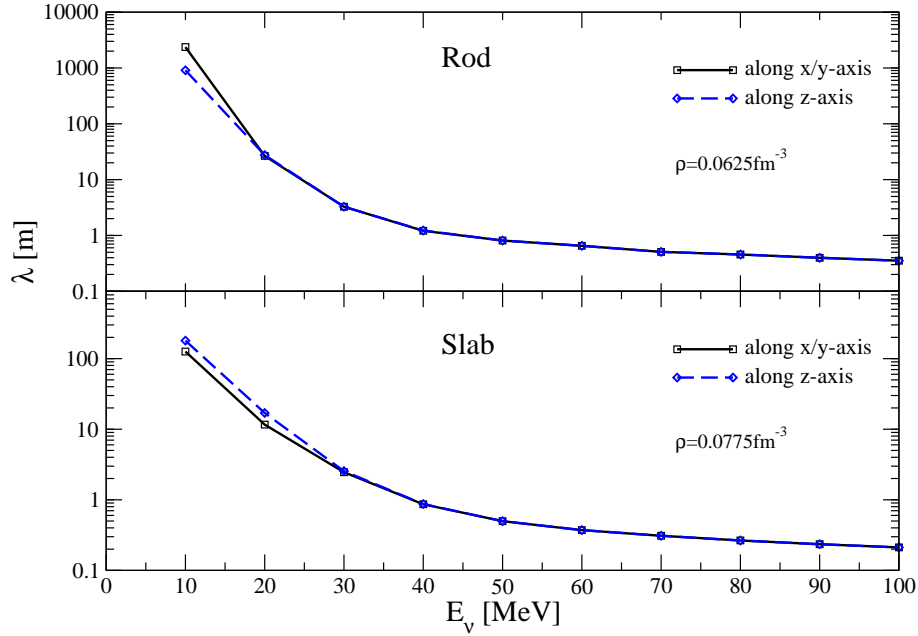


FIG. 4: The neutrino mean free path (NMFP) calculated for the charged current reaction in case of rod and slab configurations demonstrate the dependence of the result on spatial orientation of the momentum transfer \vec{q} . For these calculations we have employed results of the Skyrme HF approach and ignore the blocking of final electron states.

This can be seen from inspecting figure 3. The upper panel of this figure contains results of the proton abundances for baryonic matter in β -equilibrium resulted from non-relativistic Skyrme-Hartree-Fock calculations. The proton abundance of homogeneous matter is a monotonically increasing function of total density and it reaches the value of 4% at the density 0.1 fm^{-3} . Allowing for inhomogeneous matter distribution one obtains a significant increase of the proton fraction at densities below 0.03 fm^{-3} , while in the density region from 0.03 to 0.08 fm^{-3} its value is almost constant around 3.2%. The lower panel of figure 3 displays the corresponding results derived from the relativistic mean field approach. This relativistic approach seems to provide a smaller symmetry energy at these low densities, which leads to smaller proton abundances in the inhomogeneous as well as the homogeneous solution.

In figure 4 we want to demonstrate the dependence of the neutrino cross section for the charge current reaction on the spatial orientation of the momentum transfer \vec{q} . This is displayed in terms of the corresponding neutrino mean free path, which has been calculated according to (10) from σ_x (solid line) and σ_z (dashed line), respectively. Note that due to our choice of the coordinate system the results for σ_y are identical to those for σ_x for the

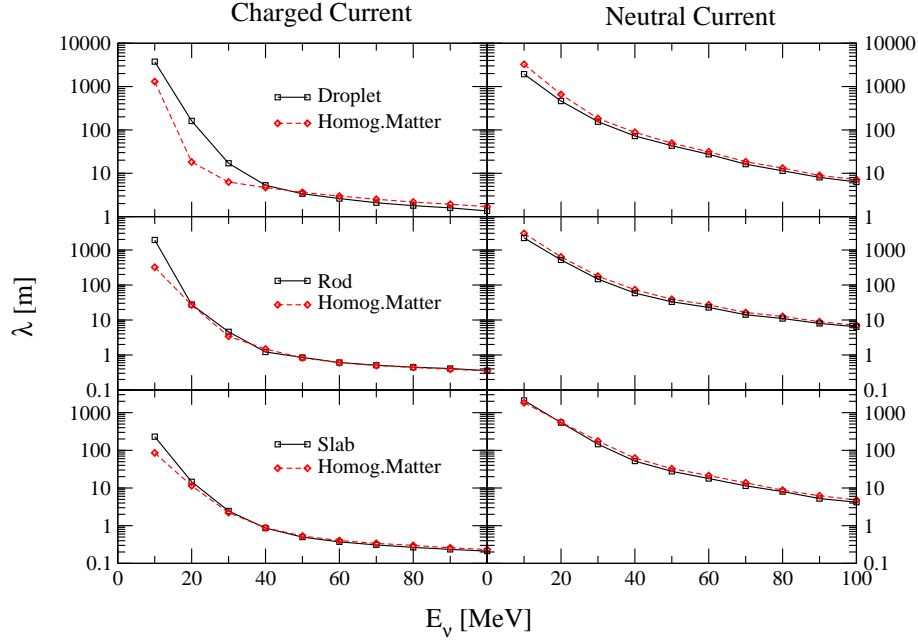


FIG. 5: Skyrme-Hartree-Fock calculations of NMFP for pasta phases (solid curves) and the respective results for homogeneous matter at the same global density (dashed curves). The results for the charged current reaction are shown in the left column, while the neutral current NMFP in the right one.

rod as well as the slab structures.

For the density ρ of 0.0625 fm^{-3} , which leads to a rod structure, we obtain results for the NMFP ranging 20 km for neutrinos with an energy of 10 MeV down to 30 cm for neutrinos with an energy of 100 MeV. For low-energy neutrinos the NMFP for reactions with a momentum transfer parallel to the x -axis is larger by a factor of 2 as compared to a momentum transfer parallel to the z -axis, difference which disappears for neutrinos with larger energies. This factor of 2 is non-negligible but small on the scale of variations for the NMFP as a function of the neutrino energy. Therefore the simple averaging procedure of (9) seems to be adequate.

Similar results are obtained for the slab configuration as can be seen from the lower panel of figure 4. Note that the results for the NMFP are considerably smaller at low neutrino energies (by a factor of 10) and even at neutrino energies as large as 100 MeV smaller by a factor 2, although the ratio of the inverse densities is only about 1.2.

The NMFP calculated in CC and NC reactions for homogeneous and inhomogeneous

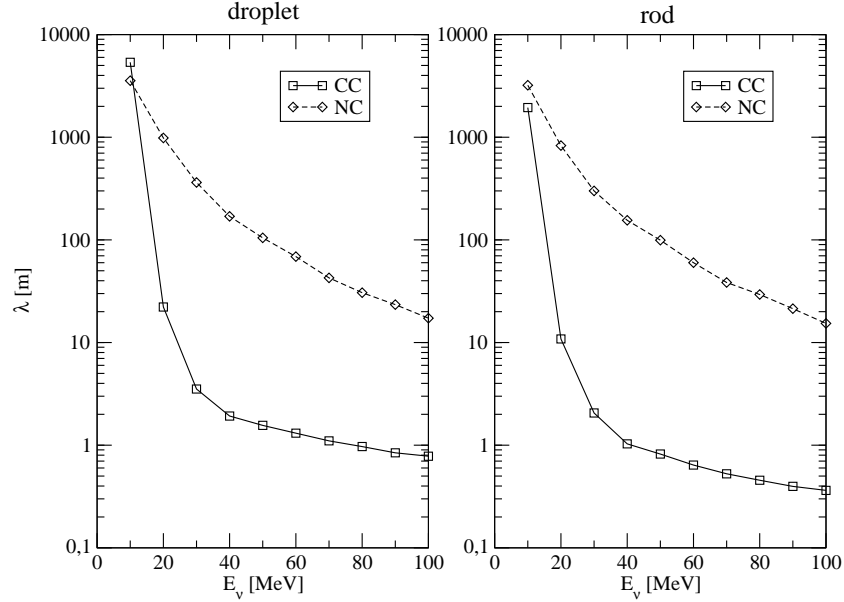


FIG. 6: Results of NMFP due to NC (dashed lines) and CC (solid lines) reactions. The description of the inhomogeneous baryonic matter distributions results from the density dependent relativistic mean-field calculations. As examples we present results for the droplet phase displayed in the left panel at a density of 0.034 fm^{-3} and for the rod phase (right panel) at 0.055 fm^{-3} .

matter distributions are shown in figure 5. First, let us compare the NMFP of homogeneous matter for both types of reactions. The main influence on NMFP's results from the available phase space for each reaction. In fact, the proton fraction of homogeneous matter does not exceed 1% for the densities considered here. Thus we have to consider a much larger blocking effect for the neutrons in the final states NC reactions than for the protons in the CC reactions. Therefore the cross section of CC absorption is larger than in NC scattering, and consequently, the mean free path is shorter, as it is shown by the red dashed lines in figure 5. Due to the small proton abundances in homogeneous matter the Pauli blocking factor of final electron states affects the result for the CC reaction only at very small neutrino energies $E_\nu < 10 \text{ MeV}$.

Figure 5 also presents results for the NMFP of inhomogeneous matter for both types of currents. First of all, we should emphasize the larger influence of electron blocking factor on CC current reaction in the droplet phase. This is due to the larger proton abundances in the β -equilibrium of the inhomogeneous matter. At a neutrino energy around $E_\nu \simeq 10 \text{ MeV}$

the mean free path of CC processes is longer in comparison with NC scattering, because in this region the Pauli blocking of electrons in CC reaction dominates over the differences in phase spaces of the baryonic states. If the energy of incoming neutrino E_ν rises the Pauli blocking drops exponentially and the ratio of the cross sections for CC and NC reactions is determined by the available phase space for the baryonic states as discussed above for the homogeneous matter calculation. This means that the NMFP of absorption due to CC becomes shorter than the respective result in NC scattering. At higher densities, where rods and slabs appear, the influence of Pauli blocking of electrons is partially compensated by the effects of the baryonic phase space. Therefore the NMFP of CC reaction remains shorter in comparison with NC reaction for all neutrinos with $10 < E_\nu < 100$.

The same features are also observed in the comparison of NMFP due to the different currents for the models of inhomogeneous baryonic matter, which are based on the relativistic mean field calculations displayed in figure 6.

The cross section for neutrino scattering in homogeneous matter increases with the baryonic density in a non-linear way (see discussion above). Therefore one may expect that the mean free path in the inhomogeneous matter is shorter than the corresponding one for homogeneous of the same global density, since the scattering on the quasi-nuclear structures shall enhance the respective cross section. Nevertheless, the NMFP obtained for the charged current reaction, which is shown in left column of figure 5 demonstrates the opposite behavior, specially at low densities, where the droplet phase occurs. The NMFP obtained from absorption in inhomogeneous matter is longer than the respective result derived from homogeneous matter calculations.

In order to explain this effect one should consider difference in proton fractions of homogeneous and inhomogeneous matter discussed in the beginning of this Section. At a typical density $0.0165 fm^{-3}$, where the droplet phase occurs the proton abundance in inhomogeneous matter is significantly larger than the respective value obtained in the homogeneous matter. This difference in the proton fractions has two effects: first, the homogeneous matter contains less protons in comparison with the inhomogeneous one. Consequently, the number of unoccupied final proton states is larger and more transitions, which contribute to the total cross section, are possible. Secondly, the chemical potential of electrons compensating the charge of the protons in matter is lower in case of homogeneous matter and the respective Pauli blocking factor for the produced electrons is lower than those obtained for the inhomogeneous matter.

geneous matter. This effect again modifies the cross section considerably at low E_ν . With increase of the energy of incoming neutrinos the Pauli blocking of electrons rapidly drops and more transitions become possible, so that the differences between homogeneous and inhomogeneous matter distributions are getting less significant and the respective NMFP's become closer one to another. At higher densities of matter, where the rod and slab phases occur, the difference in proton abundances are less important, therefore the resulted mean free paths are very similar and the effect of inhomogeneous structure becomes negligible.

At the end we should notice that at neutrino energies less than 10 MeV (thermalized neutrinos) the NMFP's of homogeneous and inhomogeneous matter distributions calculated in CC reaction significantly exceed the typical neutron star radius. Therefore one can conclude that the charged current reaction is kinematically suppressed [34].

The results of neutral current reaction are shown on the right panel of figure 5. It is obvious that the appearance of pasta phase in this case has no important influence on neutrino propagation, since this type of reaction does not depend on Pauli blocking of neutrino in final state (no trapped neutrinos). The only small difference in NMFP's of homogeneous matter and droplet phase may be explained by different values of matrix elements in (8), since the s.p. wave functions of bound neutrons in droplet significantly differ from wave functions of homogeneous matter. However even this small effect becomes negligible if the global density increases and the density profiles become smoother and transition to the homogeneous phase approaches.

A comparison of NMFP's of charged and neutral currents in case of pasta phase based on a relativistic mean-field model in a WS cell is displayed in figure 6. It is worth mentioning that within the relativistic model we could not find any formation of slab structures. Therefore only results for droplet and rod structures are shown. Also, the global density, at which the droplet phase occurs in the relativistic mean-field model is two times larger than the respective density in the nonrelativistic model. The difference between proton fractions of homogeneous matter and pasta phase is not so significant. In fact, the values of proton abundance around $\rho = 0.02 \text{ fm}^{-3}$, displayed in the lower panel of figure 3, are about 40% smaller than the corresponding values obtained in the Skyrme model (the upper panel). Therefore we omit the comparison between NMFP's of homogeneous and inhomogeneous matter however we compare the mean free paths of pasta phase for both types of reactions. One can see that at $E_\nu < 20 \text{ MeV}$ the behavior of CC curves is determined by the Pauli

blocking, while at higher energies the result becomes sensitive to the structure of phase space available for the reactions. Both charged and neutral current mean free paths decrease if the global density of matter rises.

Summarizing we conclude that the NMFP is determined by two different factors. The first of them - the Pauli blocking effect of final electrons in CC reaction play the most important role at low neutrino energy and drops exponentially if the energy increases. The second factor is the difference in baryonic phase spaces of different reactions. The phase space of CC absorption is larger than in NC scattering, because the Fermi energy of final (proton) states is considerably lower than the neutron Fermi energy.

V. SUMMARY AND CONCLUSION

The aim of this study was to examine the role of the inhomogeneous baryonic density structures in the crust of neutron stars on the propagation of neutrinos. Our calculations of neutrino mean free paths (NMFP) are based on microscopic descriptions of the so-called “pasta structures” derived from 3D Hartree-Fock calculations with the SLy4 parameterization of the Skyrme potential as well as density-dependent relativistic mean-field calculations, which reproduce the empirical properties of normal nuclei with good accuracy. We find that the evaluated NMFP due to charged current reactions significantly depend on the structure of the pasta phase. This is mainly due to fact that the proton abundances derived from the β -equilibrium in inhomogeneous matter are larger than the corresponding values determined for symmetric matter. The effects of inhomogeneous baryonic density distributions is less pronounced for the neutral current contribution.

Recent studies show that the weakly bound neutrons may play an important role in formation of collective modes in the crust of neutron stars [19]. In our calculations the role of such collective features of neutrons has not yet been considered and an accurate calculation of nuclear response functions should be done in the future.

VI. ACKNOWLEDGMENTS

One of us, P. Grygorov, would like to thank Dr. V. Rodin for useful discussions on weak interaction with nuclei. This work has been supported by the European Graduate School

“Hadrons in Vacuum, in Nuclei and Stars” (Basel, Graz, Tübingen), which obtains financial support by the DFG.

References

- [1] Tubbs D L and Schramm D N 1975 *Astrophys. J.* **201** 467
- [2] Sawyer R F 1975 *Phys. Rev. D* **11** 2740; 1989 *Phys. Rev. C* **40** 865
- [3] Iwamoto N and Pethick C J 1982 *Phys. Rev. D* **25** 313
- [4] Reddy S, Prakash M, and Lattimer J M 1998 *Phys. Rev. D* **58** 013009
- [5] Reddy S, Prakash M, Lattimer J M and Pons J A 1999 *Phys. Rev. C* **59** 2888
- [6] Navarro J, Hernández E S and Vautherin D 1999 *Phys. Rev. C* **60** 045801
- [7] Margueron J, Vidaña I and Bombaci I 2003 *Phys. Rev. C* **68** 055806
- [8] Ravenhall D G, Pethick C J and Wilson J R 1983 *Phys. Rev. Lett.* **50** 2066
- [9] Oyamatsu K 1993 *Nucl. Phys.* **A561** 431
- [10] Horowitz C J, Pérez-García M A and Piekarewicz J 2004 *Phys. Rev. C* **69** 045804
- [11] Caballero O L, Berry D K and Horowitz C J 2006 *Phys. Rev. C* **74** 065801
- [12] Watanabe G, Sato K, Yasuoka K and Ebisuzaki T 2003 *Phys. Rev. C* **68** 35806
- [13] Sonoda H, Watanabe G, Sato K, Takiwaki T, Yasuoka K and Ebisuzaki T 2007 *Phys. Rev. C* **75** 042801
- [14] Reddy S, Bertsch G and Prakash M 2000 *Phys. Lett.* **B475** 1
- [15] Burrows A, Reddy S and Thompson T A 2006 *Nucl. Phys.* **A 777** 356
- [16] Gögelein P and Muther H 2007 *Phys. Rev. C* **76** 024312
- [17] Gögelein P 2007 *PhD Thesis* University of Tübingen, Germany (unpublished)
- [18] Gögelein P, Van Dalen E N E, Fuchs C and Muther H 2007 *Phys. Rev. C* **77** 025802
- [19] Khan E, Sandulescu N and Van Giai N 2005 *Phys. Rev. C* **71** 042801
- [20] Skyrme T H R 1959 *Nucl. Phys.* **9** 615
- [21] Vautherin D and Brink D M 1972 *Phys. Rev. C* **5** 626
- [22] Bonche P and Vautherin D 1981 *Nucl Phys.* **A372** 496
- [23] Ring P and Schuck P 1980 *The Nuclear Many Body Problem* (Springer, New York) p 716

- [24] Chabanat E, Bonche P, Haensel P, Meyer J, Schaeffer R 1998 *Nucl. Phys.* **A635** 231
- [25] Bonche P, Flocard H, Heenen P -H, Krieger S J, Weiss M S 1985 *Nucl. Phys.* **A443** 39
- [26] Davies K T R, Flocard H, Krieger S and Weiss M S 1980 *Nucl. Phys.* **A342** 111
- [27] Montani F, May C and M  ther H 2004 *Phys. Rev. C* **69** 065801
- [28] Walecka J D 1975 *Muon Physics* vol. II ed Hughes V H and Wu C S (Academic, New York);
O’Connell J C, Donnelly T W, and Walecka J D 1972 *Phys. Rev. C* **6** 719 ; Donnelly T W
and Walecka J D 1976 *Nucl. Phys.* **A274** 368 ; Donnelly T W and Haxton W C 1979 *Atomic
Data Nucl. Data Tables* **23** 103
- [29] Eisenberg J M and Greiner W 1970 *Excitation Mechanisms of the Nucleus* (North-Holland
Publishing Company, Amsterdam-London) p 487
- [30] Schiller E and M  ther H 2001 *Eur. Phys. J.* **A11** 15
- [31] Hofmann F, Keil C M and Lenske H 2001 *Phys. Rev. C* **64** 034314
- [32] Van Dalen E N E, Fuchs C and Faessler A 2007 *Eur. Phys. J. A* **31** 29
- [33] Kl  hn T *et al* 2006 *Phys. Rev. C* **74** 035802
- [34] Boguta J 1981 *Phys. Lett. B* **106** 255; Lattimer J M, Pethik C J, Prakash M and Haensel P
1991 *Phys. Lett.* **66** 201